Dynamic molecular interferometer: Probe of inversion symmetry in I_2^- photodissociation

Richard Mabbs, Kostyantyn Pichugin, and Andrei Sanov[a)]
Department of Chemistry, University of Arizona, Tucson, Arizona 85721-0041

(Received 15 April 2005; accepted 17 June 2005; published online 11 August 2005)

Time-resolved photoelectron imaging of negative ions is employed to examine 780-nm dissociation dynamics of I_2^-, emphasizing the effects of interference in time-resolved photoelectron angular distributions obtained with 390-nm probe. No energetic changes are observed after about 700 fs, but the evolution of the photoelectron anisotropy persists for up to 2.5 ps, indicating that the electronic wave function of the dissociating anion continues to evolve long after the asymptotic energetic limit of the reaction has been effectively reached. The time scale of the anisotropy variation corresponds to a fragment separation of the same order of magnitude as the de Broglie wavelength of the emitted electrons ($\lambda = 35$ Å). These findings are interpreted by considering the effect of I_2^- inversion symmetry and viewing the dissociating anion as a dynamic molecular-scale "interferometer," with the electron waves emitted from two separating centers. The predictions of the model are in agreement with the present experiment and shed new light on previously published results [A. V. Davis, R. Wester, A. E. Bragg, and D. M. Neumark, J. Chem. Phys. **118**, 999 (2003)]. © *2005 American Institute of Physics*. [DOI: 10.1063/1.1997131]

I. INTRODUCTION

Representative of the spectroscopic approach in general, photoelectron spectroscopy[1,2] has traditionally focused on transition frequencies, which are related to the energy levels occupied by electrons in atoms and molecules. The recent advances in photoelectron imaging[3–6] have been driven, to a large degree, by the promise of more direct insights not only into the energetics but also the intimately related properties of the electronic wavefunctions,[7] i.e., the atomic and molecular orbitals. The properties of the wave functions, such as symmetry, spatial extent, and localization, along with the energy eigenvalues, are the core descriptors of molecular structure and, therefore, chemistry.

The dynamics of chemical reactions are effectively unraveled via direct time-resolved measurements and therefore the greatest potential of photoelectron imaging lies in its combination with femtosecond pump-probe techniques.[8] This strategy focuses on real-time evolution of the electronic structure, bringing the research to the true forefront of chemistry, as it is the electrons that control chemical bonding and ultimately determine the reaction outcomes.

In the field of negative-ion spectroscopy, the first time-resolved observation of dynamics from the electronic perspective was accomplished in the femtosecond photoelectron spectroscopy experiment of Greenblatt *et al.* investigating I_2^- photodissociation.[9] This system was revisited several times,[5,10–12] yet the main experimental focus has remained on the evolution of the energetics, including the effects of interaction between the separating fragments. This emphasis has been largely unaffected even by the introduction of the photoelectron imaging approach,[5,12] partially due to the complexity of the theory involved in the analysis and interpretation of time-resolved photoelectron angular distributions.[7] Nonetheless, Davis *et al.* did report time-dependent changes to the photodetachment anisotropy in I_2^- photodissociation.[5] Of particular note is the intriguing increase in the β_2 anisotropy parameter occurring around 650 fs, which was hypothesized to reflect the passage through a shallow polarization-induced minimum on the long-range potential, followed by a decrease in β_2, which was attributed to the electron localization.

In this work, we emphasize the effects of quantum interference on time-resolved photoelectron angular distributions in the photodissociation of I_2^-. The results indicate that the evolution of the electronic wave function of the dissociating molecular anion continues long after the asymptotic energetic limit has been effectively reached. Our excitation regime is very similar to that employed by Neumark and co-workers,[5,9] setting the stage for comparable dissociation dynamics. However, in contrast with the previous work, we probe the emergence of the asymptotic I^- fragments much closer energetically to the detachment threshold. The photoelectrons are produced with an asymptotic electron kinetic energy (eKE) of 0.12 eV, compared to 1.6 eV in the Neumark experiments. This corresponds to a significantly larger de Broglie wavelength, which we show to be a critical parameter connecting the photodissociation and electron emission dynamics.

At the heart of our findings is the effect of inversion symmetry on the electronic structure evolution in the exit channel of I_2^- dissociation. Excitation at 780 nm accesses the $A'\,1/2_g(^2\Pi)$ state and yields asymptotic $I(^2P_{3/2})+I^-$ fragments. As long as the electronic wave function of the dissociating system retains its inversion symmetry, the electron detachment is subject to interference of two equivalent emis-

[a)]Electronic mail: sanov@u.arizona.edu

sion centers, the core iodine atoms I_A and I_B, which separate at a speed determined by the reaction energetics. Hence, the dissociating I_2^- is a molecular-scale interferometer, with an arm-length R controlled by the time-dependent progress of the reaction. The emitted electron waves are sensitive probes of not only the dissociation dynamics, but also of the electron-neutral interactions, such as scattering on the neutral fragments.

In the pump-probe scheme utilized here, the I_2^- "interferometer" samples, over the span of 2–3 ps, an R range from ca. 3 Å to that similar to the 35 Å de Broglie wavelength of the photoelectrons. This sets the stage for the intriguing interplay between the fragment separation and electron emission dynamics, characterized by an easily resolvable picosecond time scale.

II. EXPERIMENTAL APPARATUS

The apparatus used in this study has been described previously.[6,12,13] In brief, it employs pulsed negative-ion generation and mass-analysis techniques,[14,15] combined with a velocity-mapped,[16] imaging[17,18] scheme for the detection of photoelectrons.

For the generation of I_2^-, the ambient vapor pressure of I_2 seeded in Ar is expanded through a pulsed nozzle (General Valve Series 9 with a Kel-F poppet) operated at a repetition rate of 70 Hz into a high-vacuum chamber with a base pressure of 10^{-6} Torr. The supersonic expansion is crossed with a 1-keV electron beam and the resulting anions are pulse extracted into a time-of-flight mass spectrometer. After the ion beam is accelerated to about 2.5 keV and focussed using an Einzel lens, it enters the detection region with a typical base pressure of $(3-5)\times 10^{-9}$ Torr. The ions are detected mass selectively using a dual-microchannel-plate (MCP) detector (Burle, Inc.) at the end of the flight tube.

The mass-selected I_2^- anions are photolyzed by the 780 -nm pump pulses and the evolving electronic structure is probed via photodetachment with 390-nm probe pulses. The regeneratively amplified Ti:sapphire laser system (Spectra Physics, Inc.) produces 1-mJ, 100-fs pulses at 780 nm. Less than half of the fundamental output is used as the pump beam, while the rest is frequency doubled in the 100-μm-thick beta barium borate (BBO) crystal of a femtosecond harmonics generator (Super Optronics, Inc.), producing $\sim$100-μJ pulses with a bandwidth of 5 nm at 390 nm. The 390-nm probe beam passes through a motorized translation stage (Newport ESP300 Universal Motion Controller) to enable controlled temporal separation of the pump and probe pulses. The pump and probe beam paths are combined before entering the reaction chamber using a dichroic beam splitter. Both laser beams are mildly focussed using a 1-m focal length lens positioned approximately 45 cm before the intersection with the ion beam. The position of zero delay and the temporal resolution are determined by overlapping the pump and probe pulses in a BBO crystal and monitoring the sum-frequency signal.

The ion and laser beams intersect at the center of the 2.5-cm-wide extraction region of the velocity-mapping[19] electrostatic lens. In previously reported experiments on I_2^- and IBr^-,[12] the potential difference across the extraction electrodes was 200 V, defining the 80-V/cm dc field used. For improved angular resolution, in the experiments reported here, the potential difference across the extraction electrodes is reduced to 100 V, corresponding to a lower, 40-V/cm dc field in the region where all photochemical events take place. The imaging lens projects the photodetached electron cloud in the direction perpendicular to the ion and laser beams. A 40-mm-diam MCP detector with a P47 phosphor screen (Burle, Inc.) is mounted at the end of an internally μ-metal-shielded electron flight tube. Images are obtained from the phosphor screen using a charge-coupled device (CCD) camera (Roper Scientific Inc.). To suppress background signals, the potential difference across the two MCPs is only pulsed up to 1.8 kV for a 200-ns-wide collection window, timed to coincide with the arrival of the photoelectrons. For the rest of each experimental cycle, the dual-MCP potential difference is maintained at 1.0–1.2 kV, which is not enough to produce a detectable signal.

Extraneous pump or probe photon detachment signals are removed using computer-controlled shutters in the pump and probe beam paths and the data acquisition and correction algorithm described previously.[13] Every data points presented in this work represent the result of 10^6–10^7 experimental cycles.

All photoelectron images collected in this work were recorded using linearly polarized pump- and probe-laser beams, with the polarization direction parallel to the imaging detector surface. The cylindrical symmetry imposed by this polarization geometry enables the reconstruction of the photoelectron velocity and angular distributions by means of the inverse Abel transformation.[18] The Abel inversion is performed with the basis set expansion (BASEX) program developed by Dribinski *et al.*[20]

III. RESULTS

The 780-nm pump, 390-nm probe photoelectron images were collected in the dissociation of I_2^- at selected delays ranging from 0 to ca. 5 ps. Representative images corresponding to 100, 550, 1650, and 2650 fs are shown in Fig. 1, right. On the left is a time-energy plot showing the evolution of the photodetachment spectrum throughout the dissociation. The plot is generated from the photoelectron spectra extracted from the individual time-resolved photoelectron images.

At $t<300$ fs, the time-energy plot in Fig. 1 reveals a narrowing of the photodetachment band, coinciding with the shift of its maximum towards smaller eKE. This is followed by a slight reverse shift to larger eKE at $t=300$–600 fs. The transient eKE dip is attributed to a shallow, 0.017 ± 0.010 eV, well on the $A'\,I_2^-$ potential with a minimum at $R=6.2$ Å, as characterized by Zanni *et al.*[11] The well arises from a long-range polarization-induced attraction between the $I(^2P_{3/2})$ $+I^-$ fragments.

The evolution of the photoelectron spectrum effectively stops after 700 fs. The plot in Fig. 1 extends to 2.85 ps, but the complete data set includes pump-probe delays of up to 5 ps, with no spectral variations observed in the extended

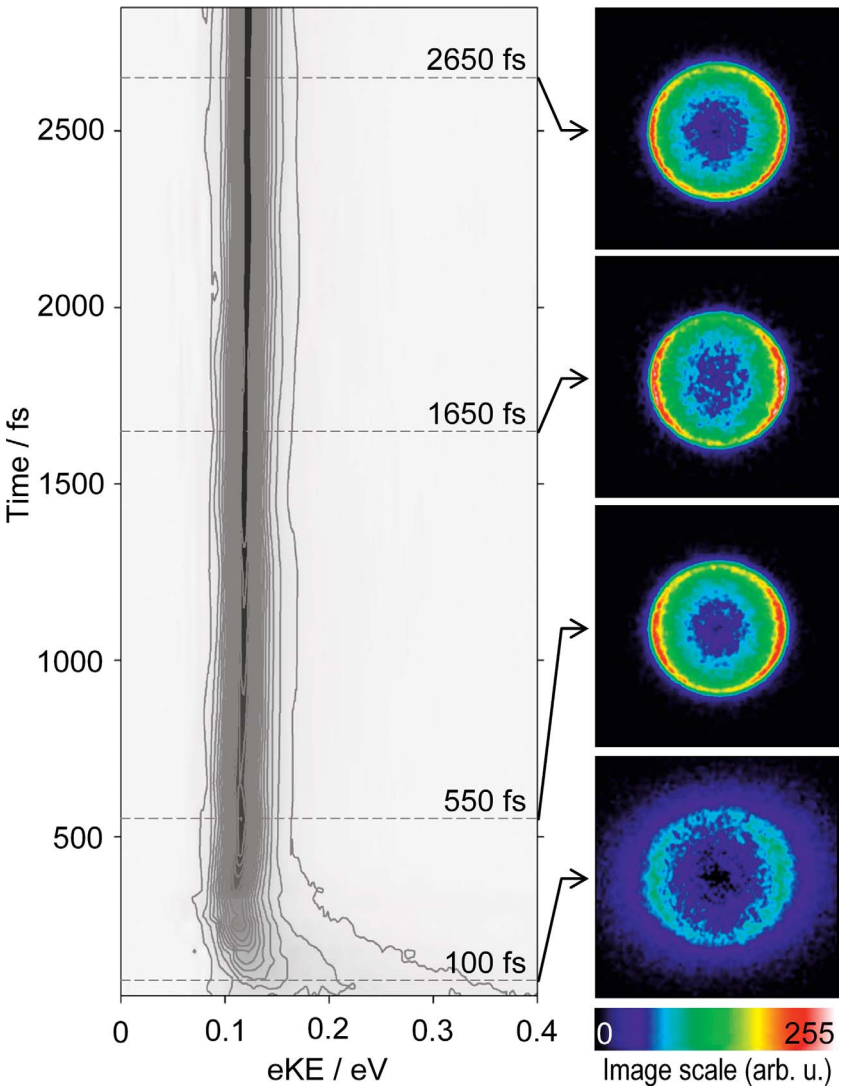

FIG. 1. (Color) Left: the time-resolved photoelectron spectrum obtained in the dissociation of I_2^- using a 780-nm pump and a 390-nm probe. The plot is generated from the photoelectron spectra extracted from the time-resolved photoelectron images. Right: representative raw photoelectron images corresponding to 100, 550, 1650, and 2650 fs (the delays are indicated by dashed lines on the time-energy plot on the left). The pump and probe polarization directions are vertical in the plane of the figure.

range. At $t>700$ fs, the peak position at eKE=0.12 eV corresponds to the difference between the probe photon energy, 3.18 eV, and the electron affinity of atomic iodine, 3.06 eV.[21] The asymptotic width of the band, 0.05 eV (full width at half maximum), reflects the probe bandwidth convoluted with other broadening factors. Overall, the time-resolved spectrum in Fig. 1 supports the conclusion by Davis *et al.* that the dissociation is effectively complete after 700 fs.[5]

Although it indeed appears that the electronic identity of the I^- fragment is established early in the dissociation, this conclusion is based on the time-resolved photoelectron spectra only. Photoelectron images contain an additional dimension of information in the angular domain and the analysis reveals that the evolution of the angular distributions continues well beyond 700 fs. For example, it can be discerned by careful inspection of Fig. 1 that the 1650-fs photoelectron image is slightly more anisotropic than both the 550- and 2650-fs images. The persisting changes in the angular distributions suggest that the evolution of the electronic wave function continues after the asymptotic energetic limit has been reached (within the experimental energy resolution). The key to unraveling these dynamics lies in the time-resolved photoelectron angular distributions—*not* the energy spectra.

The quantitative analysis of the angular distributions is summarized in Fig. 2, which displays the delay dependence of the anisotropy parameter β_2. The values of β_2 were determined by fitting the experimental time-resolved angular distributions with the equation generally describing two-photon (pump-probe) angular distributions:

$$I(\theta) = b[1 + \beta_2 P_2(\cos\theta) + \beta_4 P_4(\cos\theta)], \quad (1)$$

where $P_2(\cos\theta)$ and $P_4(\cos\theta)$ are the second- and forth-order Legendre polynomials, β_2 and β_4 are the corresponding anisotropy parameters, and b is a normalization constant. The experimental angular distributions were obtained by integrating the Abel-transformed images over the radial range corresponding to the full width (at half maximum) of the photodetachment band in the energy domain. The β_2 values plotted in Fig. 2 represent the averages over N ($N=3-10$) separate measurements under the same experimental conditions, after testing each set using Dixon's method for data sets with <25 members and rejecting any outliers.[22] The error bars represent the 95% confidence limits of the experimentally determined mean values. Data points at shorter de-

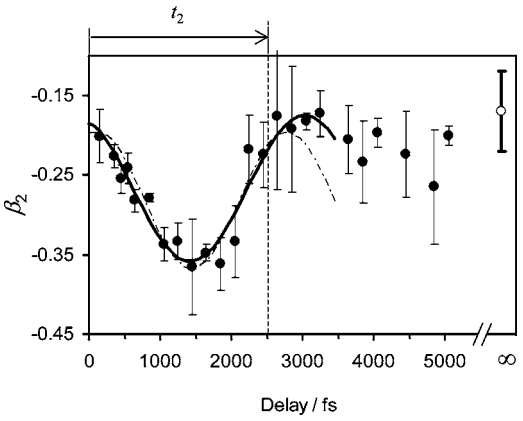

FIG. 2. Evolution of the β_2 photoelectron anisotropy parameter. Time-resolved I_2^- data are shown as solid symbols with the error bars determined as described in the text. The open symbol corresponding to "$t=\infty$" reflects the anisotropy value for the isolated I^- photodetachment. The indicated time interval t_2 corresponds to the 2.5 ps electron-localization time scale discussed in Sec. IV. The thick solid curves represents a least-squares fit to the experimental data in the $t=0-3$ ps range using Eq. (2) with a zero phase shift. The fit yields $\lambda=42.7\pm1.1$ Å for the effective de Broglie wavelength of the photoelectrons. The thin dash-dotted curve represents a fit using the same equation with the de Broglie wavelength set to its far-field value of $=35.4$ Å, while the phase-shift factor is treated as an adjustable parameter accounting for the near-field electron-fragment interactions. See the text for details.

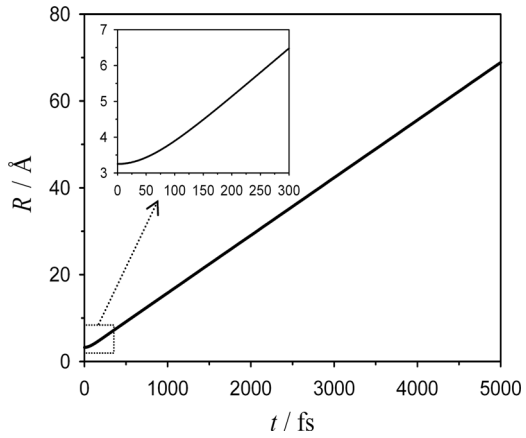

FIG. 3. The dissociation trajectory of I_2^- on the $A'\,^2\Pi_{g,1/2}$ excited-state potential accessed using the 780-nm pump. In the 0–1-ps range, the trajectory is calculated by solving the classical equation of motion as described in the text. For $t>1$ ps, linear extrapolation was used. The inset shows the expanded 0–300-fs range.

lays tend to be associated with narrower error bars, compared to longer delays, because the corresponding measurements typically include larger datasets (larger N). The overall trend in the β_2 values shown in Fig. 2 is fully repeatable.

The higher-order moment β_4 is more susceptible to experimental noise, resulting in greater, compared to β_2, errors. Hence, only the β_2 values are plotted in Fig. 2. It is stressed that the time scales apparent in the time-dependent angular distributions are adequately reflected in $\beta_2(t)$, and therefore reporting only these values is sufficient. We have also carried out the anisotropy analysis by artificially setting β_4 to zero, independent of pump-probe delay. This additional constraint changes (to a small extent) the corresponding β_2 values, yet the overall temporal trends in the data remain unaffected.

After the completion of the dissociation, the photoelectrons originate from the closed-shell I^- fragment. Therefore, the alignment with respect to the pump-laser polarization is no longer important in the asymptotic data, i.e., $\beta_4=0$, while β_2 at long pump-probe delays can be compared to that in "static" photodetachment of I^- at the same (390 nm) wavelength. The latter, $\beta_2=-0.17\pm0.05$,[23] is indicated in Fig. 2 by an open circle at $t=\infty$. The corresponding error bars reflect the 95% confidence interval determined previously[23] by modeling I^- photodetachment data at different photon energies. This interval includes not only the uncertainty of the 390-nm measurement, but also the cumulative errors attributable to other measurements, as well as theoretical modeling.

IV. DISCUSSION

A. Relevant time scales

Given the 1.01 eV bond dissociation energy,[9,10] the excitation of I_2^- at 780 nm results in a 0.58 eV kinetic energy release to the $I(^2P_{3/2})+I^-$ products, which corresponds to an asymptotic fragment separation speed of 13.3 Å/ps. Figure 3 shows the classical dissociation trajectory $R(t)$ calculated for the present case.[12] In the range of $t<1$ ps, the trajectory was propagated on the $A'\,I_2^-$ potential characterized by Zanni *et al.*[11] For $t>1$ ps, an extrapolation using the above asymptotic speed was used.

Using the above dissociation trajectory, the following time scales relevant to our experiment must be considered.

1. Change in the Σ/Π character of the A' state of I_2^-

Due to the extensive spin-orbit interaction, the A' electronic state of I_2^- is described as an admixture of Hund's case (a) Σ and Π states.[24] Although experimental measurements show that the photofragments from the $A'\leftarrow X$ transition align parallel to the laser polarization axis,[25] the A' state predicted to be predominantly ($\sim$90%) Π in character in the Franck-Condon region.[24] The state composition is bond length (R) dependent, and may therefore affect the evolution of the photoelectron angular distributions in time-resolved dissociation. By the time an internuclear separation of 5.3 Å is reached, the Σ-character component of the A' state is predicted to reach $\sim$63%, approaching the asymptotic ($R=\infty$) limit of 67%.[24] In view of these estimates and based on the dissociation trajectory in Fig. 3, the change in the Σ/Π electronic character in the dissociation process occurs on a $<$200-fs time scale, which is extremely rapid compared to the observed anisotropy variation (see Fig. 2). Hence, an alternative explanation for the observed effect must be sought.

2. de Broglie time scale

Rather than reflecting the change in the R-dependent Σ/Π composition of the excited state, it is apparent by inspection of Fig. 2 that the anisotropy parameter completes a cycle of evolution within the first 2.5–3 ps. A 2.5-ps delay corresponds to a 36-Å separation between the fragments (see Fig. 3). This length scale is a critical clue for understanding

the dynamics, as it is remarkably similar to the de Broglie wavelength of the asymptotic (eKE=0.12 eV) photoelectrons, $\lambda=35.4$ Å. Therefore, the 2.5-ps time scale, hereafter referred to as the de Broglie time scale, denoted by t_1, appears to couple the dynamics of the nuclear separation and electron emission.

3. Electron-localization time scale

On the other hand, as pointed out by Davis *et al.*,[5] the evolution of the anisotropy parameter should also reflect the change in the electronic wave-function character from that corresponding to the $A'\,^2\Pi_{g,1/2}$ molecular state to that corresponding to the excess electron localized on one of the atomic fragments. In the present experiment, the time-dependent changes in the anisotropy persist for more than 2 ps. For comparison, having examined the 793-nm dissociation of I_2^- with a 264-nm probe, Davis *et al.* suggested that the localization of the excess electron occurs by 800 fs, when the evolution of the anisotropy in their experiment stops.[5]

The likely mechanism of the localization of the excess electron on one of the fragments relies on the external-field mixing of I_2^- electronic states of *gerade* and *ungerade* symmetry, such as the $A'\,^2\Pi_{g,1/2}$ and $X\,^2\Sigma_u^+$ states.[5] In both the Neumark group's and our experiments, the photodissociation and photodetachment occur in the presence of dc fields. Comparing the 40-V/cm field used in this work to the 500-V/cm field in the experiment of Davis *et al.*,[5] the delocalized nature of the $(I\cdots I)^-$ electronic wave function is expected to persist longer in our case. This prediction is indeed seen to be in agreement with the experimental observations.

In examining the effect of the dc field, we have considered measurements with a stronger, 80-V/cm extraction field within the electron imaging lens. The corresponding images were reported previously alongside the similar measurements on IBr^-,[12] albeit without discussing the angular distributions. Although the 80-V/cm data set is less extensive compared to the present work, crude analysis of the 80-V/cm images for I_2^- and IBr^- reveals two qualitative observations relevant here. First, the anisotropy trends in the 80-V/cm I_2^- experiment are similar to the 40-V/cm data reported in the present work, with similar characteristic time scales. Second, the photodetachment anisotropy in the IBr^- case does not exhibit a significant variation on the 2.5-ps time scale observed in I_2^-, leveling off at the asymptotic I^- level much earlier in the dissociation process. For example, it can be seen by inspection of the pump-probe images in Ref. 12 (Fig. 2) that the 1350-fs I_2^- photoelectron image is more anisotropic than the 1400-fs IBr^- image, with the latter corresponding, essentially, to the asymptotic I^- limit.

A quantitative estimate of the localization time scale can be obtained as follows. For effective state mixing, the two unperturbed potential-energy curves must come close enough for the splitting to be comparable to the energy difference between the $(I_A+I_B^-)$ and $(I_A^-+I_B)$ localized-electron states in the presence of the external field. While the field-induced perturbation is of the order of $H'=eER$, where E is field intensity, a reliable estimate of the R-dependent splitting between two molecular states is quite challenging at large internuclear distances. As an estimate, we take the 0.8-meV splitting between the $A'\,^2\Pi_{g,1/2}$ and $X\,^2\Sigma_u^+$ states at $R=13$ Å, cited by Davis *et al.*,[5] and further assume that the long-range $(I\cdots I)^-$ potentials scale as R^{-4} (charge-induced-dipole interaction). Then, the g-u energy splitting can be modeled as $\Delta E=C/R^4$, where the coefficient $C=23$ eV Å^4 is chosen to reproduce the above value at $R=13$ Å. Requiring $\Delta E\approx H'$, the field-induced transition to a localized-electron state should occur at $R\approx(C/eE)^{1/5}$, which under our experimental conditions ($E=40$ V/cm) corresponds to $R\approx35.6$ Å. By sheer (unintended) coincidence, this value is very close to the de Broglie wavelength of the asymptotic photoelectrons ($\lambda=35.4$ Å).

The internuclear distance of $R=35.6$ Å needed, according to the above estimate, for the electron-localization transition is reached at 2.5 ps, which we hereafter consider as an approximate electron-localization time scale t_2.

4. The overall picture

Hence, two different in nature but similar in magnitude time scales, both coincidentally equal to 2.5 ps, are at play in the experiment: t_1, defined by the photodissociation and photodetachment energetics, and t_2, which depends on the external field.

At early stages of the dissociation, the photodetached electron is emitted from an I_2^- molecular orbital, which can be viewed as a linear combination of atomic orbitals localized on two equivalent centers, separated by time-dependent distance R. As in any interference scenario, the emitted waves are expected to reflect the variation in R/λ, where λ is the de Broglie wavelength. The corresponding time scale t_1 is the time necessary for the fragments to separate to $R\approx\lambda$, where λ is the de Broglie wavelength of the photoelectrons. Indirect support for this picture is found in the lack of significant long-range time dependence of β_2 in the case of $IBr^-\rightarrow I^-+Br$ dissociation, in which case the electron detachment does not involve two equivalent centers.

For the dissociation to complete in the I_2^- case, the excess electron must localize on one of the fragments, thus breaking the inversion symmetry. It is *not* the act of the imaging measurement that collapses the excess-electron wave function to a localized atomic orbital. In any experiment, the wave function is collapsed to one of the eigenfunctions of the operator corresponding to the type of measurement involved. In photoelectron imaging, the measurement is the determination of position of an electron impact on the detector and the corresponding eigenfunctions are delta functions of laboratory-frame coordinates—not the $5p$ orbitals localized on one of the I atoms. Hence, the photodetachment step does not localize the excess-electron wave function. Averaging over many electron impacts on the detector yields the projection of the probability density distribution corresponding to the free-electron wave function ψ_f. The properties of ψ_f are, in turn, determined by the initial (bound-) electron state, which can be either localized or delocalized in nature.

The time scale for the electron localization, t_2, is (presumably) defined by external-field mixing of the delocalized (molecular) electronic states. For the present experimental conditions, t_2 is estimated to be $\sim$2.5 ps. This crude estimate

agrees with the drop off in β_2 magnitude seen in Fig. 2. Given the similar values of the two timescales, t_1 and t_2, only the first cycle of the interference-induced anisotropy variation is expected (and seen) in the data. Due to the scaling of t_2 with the extraction field, $t_2 \propto E^{-1/5}$, the experimental grip of this parameter is not very good, for example, a factor of 2 increase in the extraction field would shorten the localization time scale by only 15%. The predicted weak dependence of t_2 on the field may explain why no significant difference is observed between the anisotropy trends in our 40- and 80 -V/cm data sets, within the combined uncertainty of both.

At $t > t_2$, the $I \cdots I^-$ internuclear distance hardly affects the emitted electron waves, as the parent electron orbital is by now localized on a single center. The corresponding photoelectron images reflect the photodetachment of the isolated I^- fragment and the values of β_2 in Fig. 2 level off within the confidence limits for I^-.

In what follows, we consider, in a semiquantitative fashion, the two-center interference that defines the detachment dynamics within the first 2.5 ps.

B. Two-center interference model

The observation of a cycling variation in β_2 on the de Broglie time scale suggests an interference picture for the photodetachment of dissociating I_2^-. Previously, we developed a conceptually similar two-center interference view of the (static) photodetachment of covalent dimer anions $(CO_2)_2^-$ and $(CS_2)_2^-$.[26] In the present case, the I_2^- $\sigma_u(5p)$ orbital, from which the electron detachment takes place, is described as a linear combination of the $5p$ orbitals of the two dissociating atoms, I_A and I_B: $\sigma_u(5p) = c(5p_A + 5p_B)$, where c is a normalization constant. The final-state electron wave function is then a linear combination of the waves emitted from I_A and I_B.

Considering that the probe wavelength is orders of magnitude greater than the length scales relevant in the experiment, the photodetachment can be discussed in the electric-dipole approximation. In addition, since at all relevant delays R is much smaller than the 390-nm probe wavelength, I_A and I_B emit waves with equal amplitudes, as long as the parent orbital preserves its *ungerade* symmetry. The evolution of the photoelectron angular distribution (PAD) then reflects the change in the relative phases accumulated by the waves from I_A and I_B, as observed in the far field. If we neglect, for the time being, the interaction between the photodetached electron and the neutral fragments, the phase difference is determined, among other factors, by the de Broglie wavelength λ and the separation between I_A and I_B, R. In the simplest model, not considering the details of the detachment process and orientation averaging, one expects the anisotropy to display periodicity with respect to R/λ, with a period determined by $\Delta(R/\lambda) = 1$.

This model immediately explains, qualitatively, why the anisotropy parameter completes a full cycle within the de Broglie time scale. In order to address the $\beta_2(t)$ behavior semiquantitatively, we model this evolution with a periodic function:

$$\beta_2(t) = a + b \cos\left(\frac{2\pi R(t)}{\lambda} + \phi\right). \tag{2}$$

Equation (2) is not intended to represent the exact functional form of $\beta_2(t)$, but merely to model the underlying time scale and periodicity. $R(t)$ is the dissociation trajectory (Fig. 3), while a and b can be used as adjustable parameters to model the experimental data. Factor ϕ accounts for any phase shift due to the interaction of the emitted electrons with the neutral fragments.

We first neglect the electron-neutral interactions, setting $\phi = 0$. In this case, the position of the first extreme of $\beta_2(t)$ defined by Eq. (2) is determined by λ. The least-squares fit of $\beta_2(t)$ with $\phi = 0$ to the experimental data in the $t = 0-3$ ps range is shown in Fig. 2 as a solid curve. The procedure yields $a = -0.267 \pm 0.006$, $b = 0.082 \pm 0.008$, and $\lambda = 42.7 \pm 1.1$ Å. The last value is compared to the 35.4 Å de Broglie wavelength of the 0.12-eV photoelectrons.

With $\phi = 0$, the sum of a and b in Eq. (2) corresponds to β_2 expected at $R = 0$. While this limit does not occur in the dissociation, it corresponds to a united-atom description of the diatomic anion, whereas the $5p_A$ and $5p_B$ orbitals overlap completely and in phase with each other. Hence, within the model framework, the $R = 0$ limit corresponds to the photodetachment from an atomic p orbital, similar to I^-. It is reassuring that the model value of $\beta_2(R=0) = a + b = -0.185 \pm 0.010$, as obtained from the above fit, is in excellent agreement with the experimental result for I^- at 390 nm, $\beta_2 = -0.17 \pm 0.05$.[23]

Comparing the model with the experiment, it is necessary to address the discrepancy between the de Broglie wavelength that best reproduces the experimental results, 42.7 Å, and the actual wavelength of 0.12-eV electrons, 35.4 Å. This discrepancy is not trivial, as $\lambda = 42.7$ Å corresponds to eKE = 0.08 eV, falling outside the full width at half maximum of the observed photodetachment band (see Fig. 1).

The discrepancy likely stems from the neglect of the interactions between the photodetached electron and the neutral fragments. The 35.4 Å wavelength is calculated in the far field, while the electron-neutral interactions affect the electron wavelength in the near field, contributing to the relative phases of the waves emitted from I_A and I_B. The effect of these interactions can be accounted for, approximately, by either treating λ in Eq. (2) as an adjustable parameter corresponding to an effective near-field wavelength or, alternatively, using a nonzero value of ϕ to account to the resulting phase shift.

The first approach corresponds to the fitting procedure outlined above, yielding $\lambda = 42.7$ Å. The longer effective wavelength of the emitted electrons, compared to the far-field limit, corresponds to a lower kinetic energy of the photoelectrons in the near field, possibly reflecting the effect of the centrifugal barrier in the photodetachment.

The second approach, introducing a nonzero phase factor in Eq. (2), is in general more accurate, but its inherent disadvantage is that ϕ is expected to depend on R. That is, in the extrapolated $R = 0$ limit we must have $\phi = 0$, corresponding to the united-atom description of I_2^-, while at $R \to \infty$ the

phase shift is expected to reach a nonzero asymptotic value. A simplified version of this approach can be considered by setting λ to its far-field value, 35.4 Å, and treating ϕ as a constant parameter, with the implicit assumption that the change in $\phi(R)$ occurs predominantly at internuclear separations shorter than those relevant to most of the present data set.

The dashed curve in Fig. 2 represents a corresponding least-squares fit to the experimental data in the 0–3-ps range, yielding $\phi=-40.9°\pm6.0°$, $a=-0.283\pm0.006$, and $b=0.086\pm0.008$. The negative value of the phase factor is consistent with the alternative description above, i.e., the lengthening of the electron wavelength in the near field. Extrapolating this approach to the united-atom limit, it is necessary to set $\phi=0$, in which case we get $\beta_2(R=0)=a+b=-0.197\pm0.010$, similar to the above effective-λ approach and once again in excellent agreement with the experimental I^- limit. Overall, the performance of the model with the electron-neutral interactions accounted for with a phase-shift factor is similar to that relying on an effective de Broglie wavelength.

The most important outcome of the admittedly crude model described here is that it correctly describes the *time scale* of the anisotropy variation in the experiment. The model parameters a and b as well as the phase factor ϕ in Eq. (2) do not affect the time scale. The time scale is controlled by the fragment separation speed [via $R(t)$] and the de Broglie wavelength of the photoelectrons. Both of these parameters are predetermined by the energetics.

Finally, it is instructive to examine the present results in light of the previous findings by Neumark and co-workers, who used a similar 793 nm excitation wavelength, but probed the evolving electronic structure with more energetic 265-nm photons. A decrease in β_2 was observed at delays up to 200 fs, followed by a transient increase peaking at 650 fs.[5] It was hypothesized that this behavior is related to the passage though the shallow polarization-induced minimum on the dissociation potential, followed by electron localization. In view of the present results, an alternative explanation can be put forth. From the 793-nm dissociation energetics, the internuclear distance corresponding to the transient maximum at $t=650$ fs is ~11 Å, comparing quite favorably with the 10 Å de Broglie wavelength of the 1.6-eV eKE photoelectrons generated by the probe. Again, the dissociation and electron emission dynamics appear to have a common characteristic parameter, that being the de Broglie wavelength. Hence, the time scale of the anisotropy evolution in the Neumark experiment can also be explained within the model outlined here.

V. SUMMARY

Time-resolved photoelectron imaging was applied to the photodissociation of I_2^- excited to the $A'\,1/2_g(^2\Pi)$ electronic state, emphasizing the effects of quantum interference in time-resolved photoelectron angular distributions. In contrast to the previous studies,[9,11,27] the emerging fragments are probed in a low electron kinetic-energy regime (eKE =0.12 eV), giving a better handle on the evolving photoelectron anisotropy and the inherent time scales.

While no change in the energetics is discerned after 700 fs, the photoelectron anisotropy exhibits what appears to be the first cycle of a variation persisting for up to 2.5 ps. Hence, the anion electronic wave function continues to evolve long after the energetic limit of the dissociation has been reached (within the energy resolution of the experiment). The observed time scale of the anisotropy variation corresponds to the internuclear separation of the same order of magnitude as the de Broglie wavelength of the emitted electrons (λ=35.4 Å). Therefore, this wavelength is a critical parameter connecting the photodissociation and electron emission dynamics.

We interpret these findings by considering the effect of I_2^- inversion symmetry on the electronic structure evolution in the dissociation. The dissociating anion is viewed, effectively, as a two-center dynamic interferometer, which samples, over the span of the dissociation process, a wide internuclear separation range. Two different in nature but similar in magnitude time scales are argued to play a role: (1) the de Broglie time scale, defined as the de Broglie wavelength of the emitted electrons divided by the fragment separation speed; and (2) the electron-localization time scale, describing the breaking of the inversion symmetry of the parent electronic wave function. The predictions of the model concerning these time scales are in good agreement with the present experiment. The resulting conceptual picture also sheds new light on the previously published results.[5]

ACKNOWLEDGMENTS

We gratefully acknowledge discussions with Professor Daniel M. Neumark. The financial support for this work is provided by the National Science Foundation (Grant No. CHE-0134631) and the Camille and Henry Dreyfus Foundation (Camille Dreyfus Teacher-Scholar Award).

[1] J. H. D. Eland, *Photoelectron Spectroscopy: An Introduction to Ultraviolet Photoelectron Spectroscopy in the Gas Phase* (Butterworths, London, 1984).
[2] K. M. Ervin and W. C. Lineberger, in *Advances in Gas Phase Ion Chemistry*, Photoelectron Spectroscopy of Negative Ions Vol. 1, edited by N. G. Adams and L. M. Babcock (JAI, Greenwich, 1992), p. 121.
[3] T. Suzuki, L. Wang, and H. Kohguchi, J. Chem. Phys. **111**, 4859 (1999).
[4] J. A. Davies, J. E. LeClaire, R. E. Continetti, and C. C. Hayden, J. Chem. Phys. **111**, 1 (1999).
[5] A. V. Davis, R. Wester, A. E. Bragg, and D. M. Neumark, J. Chem. Phys. **118**, 999 (2003).
[6] E. Surber, R. Mabbs, and A. Sanov, J. Phys. Chem. A **107**, 8215 (2003).
[7] T. Seideman, Annu. Rev. Phys. Chem. **53**, 41 (2002).
[8] A. Stolow, A. E. Bragg, and D. M. Neumark, Chem. Rev. (Washington, D.C.) **104**, 1719 (2004).
[9] B. J. Greenblatt, M. T. Zanni, and D. M. Neumark, Chem. Phys. Lett. **258**, 523 (1996).
[10] M. T. Zanni, T. R. Taylor, B. J. Greenblatt, B. Soep, and D. M. Neumark, J. Chem. Phys. **107**, 7613 (1997).
[11] M. T. Zanni, V. S. Batista, B. J. Greenblatt, W. H. Miller, and D. M. Neumark, J. Chem. Phys. **110**, 3748 (1999).
[12] R. Mabbs, K. Pichugin, and A. Sanov, J. Chem. Phys. **122**, 174305 (2005).
[13] R. Mabbs, K. Pichugin, E. Surber, and A. Sanov, J. Chem. Phys. **121**, 265 (2004).
[14] M. A. Johnson and W. C. Lineberger, in *Techniques for the Study of Ion*

Molecule Reactions, Pulsed Methods for Cluster Ion Spectroscopy, edited by J. M. Farrar and W. H. Saunders, Jr. (Wiley, New York, 1988), p. 591.
[15] M. E. Nadal, P. D. Kleiber, and W. C. Lineberger, J. Chem. Phys. **105**, 504 (1996).
[16] A. T. J. B. Eppink and D. H. Parker, Rev. Sci. Instrum. **68**, 3477 (1997).
[17] D. W. Chandler and P. L. Houston, J. Chem. Phys. **87**, 1445 (1987).
[18] A. J. R. Heck and D. W. Chandler, Annu. Rev. Phys. Chem. **46**, 335 (1995).
[19] A. T. J. B. Eppink and D. H. Parker, Rev. Sci. Instrum. **68**, 3477 (1997).
[20] V. Dribinski, A. Ossadtchi, V. A. Mandelshtam, and H. Reisler, Rev. Sci. Instrum. **73**, 2634 (2002).
[21] *CRC Handbook of Chemistry and Physics*, 84th ed. (CRC, Boca Raton, FL, 2004).
[22] G. W. Snedecor and W. G. Cochran, Statistical Methods, 7th ed. (Iowa State University Press, Ames, Iowa, 1980), p. 507.
[23] R. Mabbs, E. Surber, and A. Sanov, J. Chem. Phys. **122**, 054308 (2005).
[24] P. E. Maslen, J. Faeder, and R. Parson, Chem. Phys. Lett. **263**, 63 (1996).
[25] J. M. Papanikolas, V. Vorsa, M. E. Nadal, P. J. Campagnola, H. K. Buchenau, and W. C. Lineberger, J. Chem. Phys. **99**, 8733 (1993).
[26] R. Mabbs, E. Surber, and A. Sanov, Chem. Phys. Lett. **381**, 479 (2003).
[27] B. J. Greenblatt, M. T. Zanni, and D. M. Neumark, Science **276**, 1675 (1997).